Copyright © 2012 Tech Science Press CMES, vol.83, no.2, pp.143-167, 2012

Stochastic Finite Element Analysis and Reliability Of Steel Telecommunication Towers

M.M. Kamiński[1] **and J. Szafran**[1]

Abstract: The main issue in this article is computational probabilistic analysis and reliability assessment of the steel telecommunication towers subjected to material and environmental uncertainty. Such a discussion is important since very wide, frequent and relatively modern application of these structures, which are subjected to various sources of uncertainty and having at this moment no rich and time-dependent failure evidence. Numerical analysis is based on the generalized stochastic perturbation technique implemented as the Stochastic Finite Elements using the Response Function Method applied with the use of computer algebra system. A simultaneous usage of the engineering FEM system and mathematical package enables for a visualization of up to the fourth central probabilistic moments and characteristics for the structural maximum internal forces and eigenvibrations. The reliability index determination is provided using the First Order Reliability Method following directly the statements of Eurocode 0, and the external loadings are applied on the structures analyzed after other Eurocodes, but may follow other engineering codes as well. The proposed numerical technique may find its application in the stochastic forced vibrations of telecommunication towers, where physical parameters as well as the excitation spectrum may be defined as polynomial time series, for instance.

Keywords: Stochastic Finite Element method, reliability analysis, response function method, stochastic perturbation technique, symbolic computing.

1 Introduction

Probabilistic methods described widely in the literature [Lin (1967), Elishakoff (1983), Kleiber and Hien (1992), Kamiński (2005)] have still an increasing impact on the solution of the engineering problems, which is reflected now even in the engineering codes, like these applied in civil engineering at least. Structural analysis

[1] Department of Steel Structures, Faculty of Civil Engrg., Arch. & Env. Engrg., Technical University of Lodz, 90-924 Lodz, Al. Politechniki 6, Poland, Marcin.Kaminski@p.lodz.pl

accounting for the parameters uncertainty enables for computational modeling of the problems in designing, optimization and, first of all, reliability assessment of the civil engineering structures. An uncertainty of the parameters decisive for the structure's effort may have quite different sources, like structural defects, material degradation, manufacturing and erecting inaccuracies as well as geometrical imperfections and physical parameters, of course. A variety of the external loadings acting on the external parts of the buildings and skeletal structures' elements during the entire calendar year also exhibit significant random fluctuations and these are temperature's fluctuations, ice covers and wind pressure; some of these structures subjected to the vibrations may be also very sensitive to their randomness. We can mention here that at least the ice covers caused many serious failures in civil engineering in northern regions, like energetic lines in Canada. An uncertainty of some loadings' types, especially recently in the view of frequently observed weather fluctuations, seems to be very important designing issue for the civil engineers; there is no doubt that the steel skeletal telecommunication towers belong to this class of structures [Wahba et al. (1998), El-Fashny et al. (1999), Khan et al. (2004), De Oliveira (2005,2007), Nielsen (2009), Fengli et al. (2010)].

On the other hand, we have a series of the very extended and well documented mathematical-numerical models accounting for the designing parameters' randomness into the static and/or dynamic problems' structural analysis [Śniady (1988), Benaroya (1992), Schueller (2009), Kamiński (2009), Chen (2005), Ohkubo et al. (2011)] – starting from the analytical methods containing spectrum analysis, through the Monte-Carlo simulation and various perturbation methods until the stochastic polynomial expansions and representations of random parameters, where the simulation method serves usually as the comparative technique. Statistical convergence of this technique obtained for the increasing number of the repetitive computational experiments may be relatively easily generated with any engineering computer software and the only issue is the total time and computer power consumption [Bendat and Piersol (1971), Boswell (1993)]. The alternative method proposed in this paper belongs to the stochastic perturbation methods – is based on the polynomial representation of the desired output parameter with respect to some random input [Kamiński (2011)]. Numerical recovery of this function (or these functions in its local version) is provided through the series of classical FEM experiments and the Least Squares Method (LSM) carried out in the desired FEM system, while probabilistic moments and coefficients are calculated in the computer algebra system using the perturbation-based equations (MAPLE, v. 13). It is necessary to underline that a derivation of the specific analytical formulas for these output random quantities is an inherent part of the stochastic perturbation method, quite contrary to the simulation technique, where statistical estimators have quite

general character, independent from the problem being solved.

Computational experiments provided in this paper strictly concern the steel skeletal telecommunication towers with a relatively large height (around 40-60 meters), where internal structure is the 3D combination of the Euler beams and typical bars. These are the structures of a special destination giving a structural support and mounting platform for modern telecommunication equipment – antennas, cables etc. enormously expanding in the last two decades. A recent progress of the telecommunication technology resulting in the exponentially growing cell phones world and their new capabilities enforces the engineers and scientists to optimize the structures of telecommunications towers. A communication in-between particular base stations (a single tower) being the nodes of the entire telecommunication network will be in the nearest future enriched with small windmills and connected with the optical fibers and cables, so that the compressed data instead of a human voice would be transmitted around. An introduction of the highest and highest frequencies for the broadcasted signal will result in a decrease of the regions covered by a signal from a single tower and since that the total number of these towers will have to increase and a final weight of the telecommunication equipment will change also. A minimization of the final manufacturing and erection costs will remain the most important issue for the network operators, so that an introduction of still more advanced mathematical methods and software in computational mechanics accounting for the structural uncertainty is the very actual problem. This article contains a series of computational experiments documenting an influence of the randomness in various loads (like ice, temperature and static equivalent of the wind pressure) and physical characteristics (Young modulus of the stainless steel) on static behavior and eigenvibrations of the few towers showing numerical and graphical capabilities of the hybrid technique proposed.

2 Governing equations

Let us consider the following linear elasto-dynamic problem consisting of the equations of motion

$$\mathbf{D}^{\mathbf{T}}\boldsymbol{\sigma}+\tilde{\tilde{\mathbf{f}}}=\rho\ddot{\mathbf{u}}, \quad \mathbf{x}\in\Omega, \quad \tau\in[t_0,\infty), \tag{1}$$

the constitutive equations

$$\boldsymbol{\sigma}=\mathbf{C}\boldsymbol{\varepsilon}, \quad \mathbf{x}\in\Omega, \quad \tau\in[t_0,\infty), \tag{2}$$

the geometric equations

$$\boldsymbol{\varepsilon}=\mathbf{D}\mathbf{u}, \quad \mathbf{x}\in\Omega, \quad \tau\in[t_0,\infty), \tag{3}$$

the displacement boundary conditions

$$\mathbf{u} = \tilde{\tilde{\mathbf{u}}}, \quad \mathbf{x} \in \partial\Omega_u, \quad \tau \in [t_0, \infty), \tag{4}$$

the stress boundary conditions

$$\mathbf{n}\sigma = \tilde{\tilde{\mathbf{t}}}, \quad \mathbf{x} \in \partial\Omega_\sigma, \quad \tau \in [t_0, \infty), \tag{5}$$

the initial conditions

$$\mathbf{u} = \tilde{\tilde{\mathbf{u}}}^{\mathbf{0}}, \quad \dot{\mathbf{u}} = \dot{\tilde{\tilde{\mathbf{u}}}}^{\mathbf{0}}, \quad \tau = t_0. \tag{6}$$

It is assumed that all the state functions appearing in this system are sufficiently smooth functions of the independent variables $\mathbf{x}$ and τ. Let us consider the variation $\mathbf{u}(\mathbf{x}, \tau)$ in some time moment $\tau = t$ denoted by $\delta\mathbf{u}(\mathbf{x}, \tau)$. Using the above equations one can show that

$$-\int_{\Omega} (\mathbf{D}^{\mathbf{T}}\boldsymbol{\sigma} + \tilde{\tilde{\mathbf{f}}} - \rho\ddot{\mathbf{u}})^{\mathbf{T}} \delta\mathbf{u} d\Omega + \int_{\partial\Omega_\sigma} (\mathbf{n}\sigma - \tilde{\tilde{\mathbf{t}}})^{\mathbf{T}} \delta\mathbf{u} d(\partial\Omega) = 0. \tag{7}$$

Assume further that the displacement function $\mathbf{u}(\mathbf{x},\mathbf{t})$ has known values at the initial moment $\mathbf{u}(\mathbf{x}, t_1) = 0$ and at the end of the process $\mathbf{u}(\mathbf{x}, t_2) = 0$, so that the variations of this function also equal 0 at these time moments, which means $\delta\mathbf{u}(\mathbf{x}, t_1) = 0$, $\delta\mathbf{u}(\mathbf{x}, t_2) = 0$. Integrating by parts we can obtain that

$$\int_{\mathbf{t_1}}^{\mathbf{t_2}} [\delta T - \int_{\mathbf{\Omega}} \boldsymbol{\sigma}^{\mathbf{T}} \delta\boldsymbol{\varepsilon} d\Omega + \int_{\mathbf{\Omega}} \tilde{\tilde{\mathbf{f}}}^{\mathbf{T}} \delta\mathbf{u} d\Omega + \int_{\partial\mathbf{\Omega}} \tilde{\tilde{\mathbf{t}}}^{\mathbf{T}} \delta\mathbf{u} d(\partial\Omega)] d\tau = 0, \tag{8}$$

where the kinetic energy of the region Ω is defined as

$$T = \frac{1}{2} \int \rho \dot{\mathbf{u}}^{\mathbf{T}} \dot{\mathbf{u}} d\Omega. \tag{9}$$

We notice also that

$$\delta\boldsymbol{\varepsilon} = \mathbf{D}\delta\mathbf{u}, \quad \mathbf{x} \in \Omega, \quad \tau \in [t_0, \infty). \tag{10}$$

Next, we assume that the mass forces $\tilde{\tilde{\mathbf{f}}}$ and the surface loadings $\tilde{\tilde{\mathbf{t}}}$ are independent from the displacement vector $\mathbf{u}$ and, therefore, Eq. (8) can be modified to the following statement:

$$\delta \int_{t_1}^{t_2} (T - J_p) d\tau = 0 \tag{11}$$

where J_p means potential energy stored in the entire domain Ω

$$J_{\mathbf{p}} = U - \int_{\Omega} \tilde{\hat{\mathbf{f}}}^{\mathbf{T}} \mathbf{u} d\Omega - \int_{\partial\Omega_{\boldsymbol{\sigma}}} \tilde{\hat{\mathbf{t}}}^{\mathbf{T}} \mathbf{u} d(\partial\Omega) = 0 \tag{12}$$

whereas U is the elastic strain energy given by the formula

$$U = \frac{1}{2} \int_{\Omega} \boldsymbol{\varepsilon}^{\mathbf{T}} \mathbf{C} \boldsymbol{\varepsilon} d\Omega. \tag{13}$$

It is well known that Eq. (11) represents the Hamilton principle widely used in structural dynamics as the basis for further Finite Element Method and its stochastic counterpart implementations.

3 Computational implementation

Let us consider a discretization of the displacement field $\mathbf{u}(\mathbf{x}, \tau)$using the following forms [Bathe (1996), Hughes (2000)]:

$$\mathbf{u}^{\alpha}(\mathbf{x},\tau) \cong \varphi(\mathbf{x})\ \mathbf{q}^{\alpha}(\tau), \quad \mathbf{u}^{\alpha}(\mathbf{x},\tau) \cong \boldsymbol{\Phi}(\mathbf{x})\ \mathbf{r}^{\alpha}(\tau) \tag{14}$$

where $\mathbf{q}$ is a vector of the generalized coordinates for the considered finite element, $\mathbf{r}$ is a vector for the generalized coordinates of the entire discretized system. The generalized coordinates vector for the entire structure model is composed from the finite element degrees of freedom and the transformation matrix as

$$\mathbf{r}^{\alpha} = \mathbf{a}\mathbf{q}^{\alpha} \tag{15}$$

ϕ and $\boldsymbol{\Phi}$ are the corresponding shape function matrices (local and global). Contrary to the classical formulations of both FEM and the perturbation-based Stochastic Finite Element Method [Kleiber and Hien (1992)], we introduce here the additional index α=1,...,M to distinguish between various solutions of the elastodynamic problem necessary to build up the response function. The strain tensor can be expressed as

$$\boldsymbol{\varepsilon}^{\alpha}(\mathbf{x},\tau) = \mathbf{B}(\mathbf{x})\ \mathbf{q}^{\alpha}(\tau) = \tilde{\mathbf{B}}(\mathbf{x})\ \mathbf{r}^{\alpha}(\tau). \tag{16}$$

The discretized version of the Hamilton's principle is obtained as

$$\delta \int_{t_1}^{t_2} \left(\frac{1}{2} \sum \mathbf{q}^{\alpha T} \mathbf{m}^{\alpha} \mathbf{q}^{\alpha} - \frac{1}{2} \sum \mathbf{q}^{\alpha T} \mathbf{k}^{\alpha} \mathbf{q}^{\alpha} + \sum \mathbf{Q}^{\alpha T} \mathbf{q}^{\alpha} \right) d\tau = 0 \tag{17}$$

where a summation is made along with all finite elements in the system, so that we have in a global description

$$\delta \int_{t_1}^{t_2} \left(\frac{1}{2} \dot{\mathbf{r}}^{\alpha T} \mathbf{M}^{\alpha} \dot{\mathbf{r}}^{\alpha} - \frac{1}{2} \mathbf{r}^{\alpha T} \mathbf{K}^{\alpha} \mathbf{r}^{\alpha} + \mathbf{R}^{\alpha T} \mathbf{r}^{\alpha} \right) d\tau = 0, \tag{18}$$

and where the global mass matrix and stiffness matrix are defined as

$$\mathbf{M}^{\alpha} = \int_{\Omega} \rho^{\alpha}(\mathbf{x}) \tilde{\mathbf{B}}^{T}(\mathbf{x}) \tilde{\mathbf{B}}(\mathbf{x}) d\Omega, \quad \mathbf{K}^{\alpha} = \int_{\Omega} \tilde{\mathbf{B}}^{T} \mathbf{C}^{\alpha} \tilde{\mathbf{B}} d\Omega \tag{19}$$

and since the 3D bar and beam elements are used in further computations (linearly depending on Young modulus), only the first partial derivatives differ from 0. Hence, Eq. (18) can be rewritten as

$$\dot{\mathbf{r}}^{\alpha \mathbf{T}} \mathbf{M}^{\alpha} \delta \mathbf{r} - \int_{t_1}^{t_2} (\ddot{\mathbf{r}}^{\alpha \mathbf{T}} \mathbf{M}^{\alpha} + \mathbf{r}^{\alpha \mathbf{T}} \mathbf{K}^{\alpha} - \mathbf{R}^{\alpha \mathbf{T}}) \delta \mathbf{r} \, d\tau = 0. \tag{20}$$

Considering the assumptions that $\delta \mathbf{r}(t_1) = 0$, $\delta \mathbf{r}(t_2) = 0$, we finally obtain the dynamic equilibrium system

$$\mathbf{M}^{\alpha} \ddot{\mathbf{r}}^{\alpha} + \mathbf{K}^{\alpha} \mathbf{r}^{\alpha} = \mathbf{R}^{\alpha} \tag{21}$$

which represents the equations of motion of the discretized system. Once we complete this equation with the component $\mathbf{C}^{\alpha} \mathbf{r}^{\alpha}$ by getting

$$\mathbf{M}^{\alpha} \ddot{\mathbf{r}}^{\alpha} + \mathbf{C}^{\varepsilon} \dot{\mathbf{r}}^{\alpha} + \mathbf{K}^{\alpha} \mathbf{r}^{\alpha} = \mathbf{R}^{\alpha} \tag{22}$$

then we decompose the damping matrix as $\mathbf{C}^{\alpha} = \alpha_0 \mathbf{M}^{\alpha} + \alpha_1 \mathbf{K}^{\alpha}$, so that

$$\mathbf{M}^{\alpha} \ddot{\mathbf{r}}^{\alpha} + \alpha_0 \mathbf{M}^{\alpha} \dot{\mathbf{r}}^{\alpha} + \alpha_1 \mathbf{K}^{\alpha} \dot{\mathbf{r}}^{\alpha} + \mathbf{K}^{\alpha} \mathbf{r}^{\alpha} = \mathbf{R}^{\alpha}, \tag{23}$$

where no summation over the doubled indices α is applied here. As it is known, the case of the undamped free vibrations leads to the following algebraic system:

$$\mathbf{M}^{\alpha} \ddot{\mathbf{r}}^{\alpha} + \mathbf{K}^{\alpha} \mathbf{r}^{\alpha} = \mathbf{0} \tag{24}$$

and the solution $\mathbf{r}^{\alpha} = \mathbf{A}^{\alpha} \sin \omega_{\alpha} t$ leads to the relation

$$-\mathbf{M}^{\alpha} \mathbf{A}^{\alpha} \omega_{\alpha}^2 \sin \omega_{\alpha} t + \mathbf{K}^{\alpha} \mathbf{A}^{\alpha} \sin \omega_{\alpha} t = \mathbf{0}, \tag{25}$$

so that for $\sin \omega_\alpha t \neq \mathbf{0}$ and $\mathbf{A}^\alpha \neq \mathbf{0}$ there holds

$$-\mathbf{M}^\alpha \omega_\alpha^2 + \mathbf{K}^\alpha = \mathbf{0}. \tag{26}$$

Some alternative methods for determination of the eigenvalues of engineering systems with random parameters can be found in [Pradlwarter et al. (2002)]. Obviously, Eq. (22) for the time independent generalized coordinates returns the well known linear statics equilibrium systems for the RFM as follows

$$\mathbf{K}^\alpha \mathbf{r}^\alpha = \mathbf{R}^\alpha. \tag{27}$$

Let us introduce next the random variable $b \equiv b(\omega)$ with its probability density function as $p(b)$. The mth central probabilistic moment is defined as

$$\mu_m(b) = \int_{-\infty}^{+\infty} (b - E[b])^m p(b)\, db. \tag{28}$$

The basic idea of the stochastic perturbation approach is to expand all the input variables and the state functions via Taylor series about their spatial expectations using some small parameter ε>0. In case of random quantity e=$e(b)$, the following expression is employed:

$$e = e^0 + \sum_{n=1}^{\infty} \frac{1}{n!} \varepsilon^n \frac{\partial^n e}{\partial b^n} (\Delta b)^n, \tag{29}$$

where $\varepsilon \Delta b = \varepsilon \left(b - b^0\right)$ is the first variation of b about b^0, where symbol $(.)^0$ represents the function value (.) taken at the expectation b^0. Let us analyze further the expected values of any state function $f(b)$ defined according to Eq. (29) by its expansion via Taylor series with a given small parameter ε (taken as equal to 1 in numerous practical computations) as follows:

$$E[f(b)] = \int_{-\infty}^{+\infty} f(b) p(b)\, db = \int_{-\infty}^{+\infty} \left(f^0 + \sum_{n=1}^{\infty} \frac{1}{n!} \varepsilon^n \frac{\partial^n f}{\partial b^n} \Delta b^n \right) p(b)\, db. \tag{30}$$

From the numerical point of view, the expansion introduced by Eq. (30) is carried out for the summation over the finite number of components and finite limits in the integration. Now, let us focus on an analytical derivation of the probabilistic moments for the structural response function. It is easy to prove that the general 10^{th} order expansion results in the formula

$$E[f(b)] = f^0(b)|_{b=b^0} + \frac{1}{2}\varepsilon^2 \mu_2(b) \frac{\partial^2 f}{\partial b^2}|_{b=b^0} + \ldots + \frac{1}{10!}\varepsilon^{10} \mu_{10}(b) \frac{\partial^{10} f}{\partial b^{10}}|_{b=b^0}$$

(31)

where the even components in case of Gaussian variables are dropped off. Thanks to such an extension of the random output, any desired efficiency of the expected values as well as higher probabilistic moments can be achieved by an appropriate choice of the distribution parameters. Similar considerations lead to the analogous expression for a variance

$$\begin{aligned} Var\left(f\left(b\right)\right) =& \varepsilon^2 \mu_2\left(b\right) \frac{\partial f}{\partial b} \frac{\partial f}{\partial b} + \varepsilon^4 \mu_4\left(b\right) \left(\frac{1}{4} \frac{\partial^2 f}{\partial b^2} \frac{\partial^2 f}{\partial b^2} + \frac{2}{3!} \frac{\partial f}{\partial b} \frac{\partial^3 f}{\partial b^3} \right) \\ &+ \varepsilon^6 \mu_6\left(b\right) \left(\left(\frac{1}{3!} \right)^2 \frac{\partial^3 f}{\partial b^3} \frac{\partial^3 f}{\partial b^3} + \frac{1}{4!} \frac{\partial^4 f}{\partial b^4} \frac{\partial^2 f}{\partial b^2} + \frac{2}{5!} \frac{\partial^5 f}{\partial b^5} \frac{\partial f}{\partial b} \right). \end{aligned} \tag{32}$$

The third order probabilistic moment has essentially longer expansion which is shortened here to the fourth and sixth order components as

$$\mu_3\left(f\left(b\right)\right) \cong \frac{3}{2} \varepsilon^4 \mu_4\left(b\right) \left(\frac{\partial f}{\partial b} \right)^2 \frac{\partial^2 f}{\partial b^2} + \frac{1}{8} \varepsilon^6 \mu_6\left(b\right) \left(\frac{\partial^2 f}{\partial b^2} \right)^3, \tag{33}$$

Similarly, the fourth probabilistic moment is simply represented as

$$\mu_4\left(f\left(b\right)\right) \cong \varepsilon^4 \mu_4\left(b\right) \left(\frac{\partial f}{\partial b} \right)^4 + \frac{3}{2} \varepsilon^6 \mu_6\left(b\right) \left(\frac{\partial f}{\partial b} \frac{\partial^2 f}{\partial b^2} \right)^2 + \frac{1}{16} \varepsilon^8 \mu_8\left(b\right) \left(\frac{\partial^2 f}{\partial b^2} \right)^4. \tag{34}$$

Finally, one may recover the kurtosis and the skewness as

$$\kappa\left(f\left(b\right)\right) = \frac{\mu_4\left(f\left(b\right)\right)}{\sigma^4\left(f\left(b\right)\right)} - 3, \quad \theta\left(f\left(b\right)\right) = \frac{\mu_3\left(f\left(b\right)\right)}{\sigma^3\left(f\left(b\right)\right)} \tag{35}$$

and, independently, the Cornell reliability index for the particular state functions as [25]

$$\beta\left(f\left(b\right)\right) = \frac{E\left[\hat{f} - f_\alpha\right]}{\sqrt{Var\left(\hat{f} - f_\alpha\right)}} \tag{36}$$

where the pair $\left(\hat{f}; f_\alpha\right)$ denotes the real value of the given state function and its admissible counterpart.

4 Computational experiments

4.1 The tower with random Young modulus and h=52,0 m

The first numerical case is the telecommunication tower with the height equal to 52,0 meters shown schematically in Fig. 1, which illustrates the existing structure discretized in FEM computations using 63 two-noded linear elastic beam elements (legs, designed with the full circular cross sections) and 120 two-noded bars connected all in 67 nodes (rebars, taken as the angle profiles).

The structure is subjected in numerical tests to the dead load and the additional vertical forces resulting from antennas, their cables, technological platforms and their supports as well as to the technological loadings specified by the Eurocodes. The input random variable of this problem is Young modulus having expectation equal to E=205 GPa and the coefficient of variation belonging to the interval $\alpha \in [0.0,0.3]$; it is assumed to have truncated Gaussian distribution as the restricted to the positive values only. Usually, this coefficient is taken as smaller or equal to 0.15, however this enormous upper bound is driven here by the computational aspects only. The engineering FEM system is used to determine the first few eigenfrequencies using the subspace iteration algorithm, which are transferred next to the system MAPLE for further probabilistic computations. Polynomial approximation of the interrelations in-between the particular eigenvalues and Young modulus, necessary for determination of the partial derivatives in Eqs. (31-34) was provided using 9 points least squares smoothing procedure with equidistant subdivision of the Young modulus variability interval (plus minus 50% of the mean value). The final response functions were obtained as the very smooth on the entire domains, without any local oscillations, so that the partial differentiation of up to the tenth order was quite straightforward and reliable.

Figure 2 contains the 2^{nd}, 4^{th}, 6^{th} and 8^{th} order perturbation-based approximation of the first eigenvalue ($E[f_1]$, left diagram) and the fourth one ($E[f_4]$, a graph on the right). It is apparent that almost independently from analysis order all the expectations nonlinearly decrease together with an increase of the input coefficient of variation. The expected values for both eigenfrequencies are independent from the order of the stochastic perturbation method for $\alpha \in [0.0,0.1]$ and for this interval the second order technique is quite satisfactory.

These expectations asymptotically tend to the highest order curves for larger values of this coefficient (they have all concave character), where the higher input coefficient of variation, the larger differences in-between various orders' results here. Anyway, the scale of vertical axis shows that all these differences are relatively small, as measured with promiles of the final expected value. The variances shown in Fig. 3 are also collected for the first ($Var[f_1]$, left graph) and fourth eigenvalue

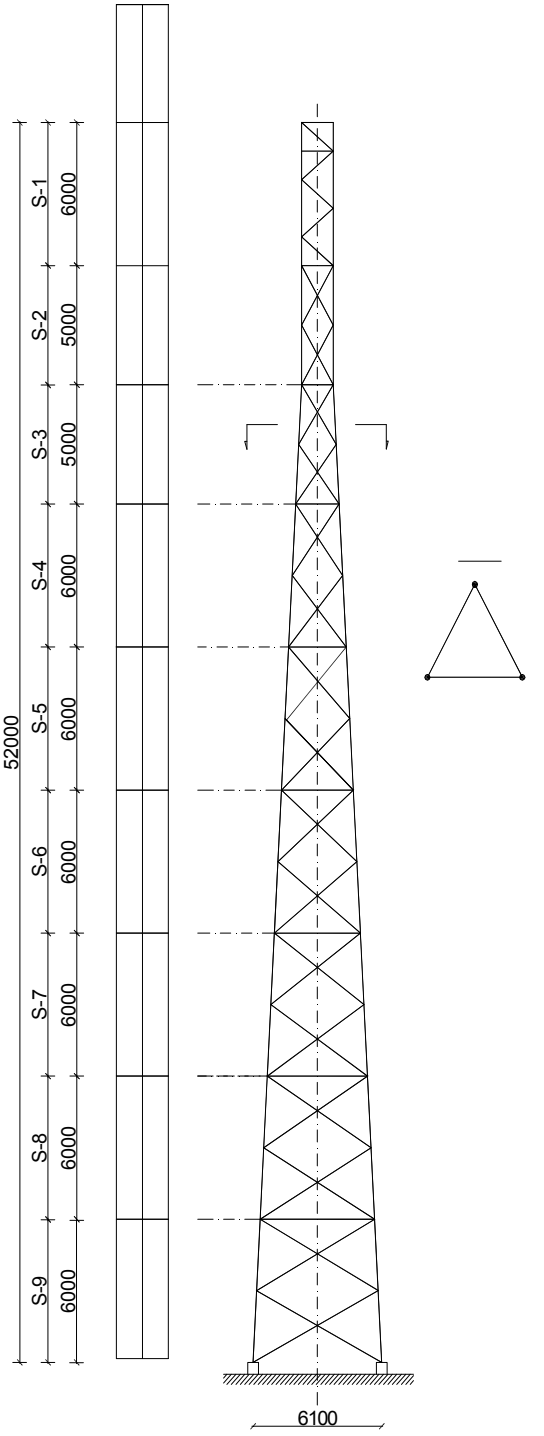

Figure 1: Static scheme of telecommunication tower with a height of 52 m

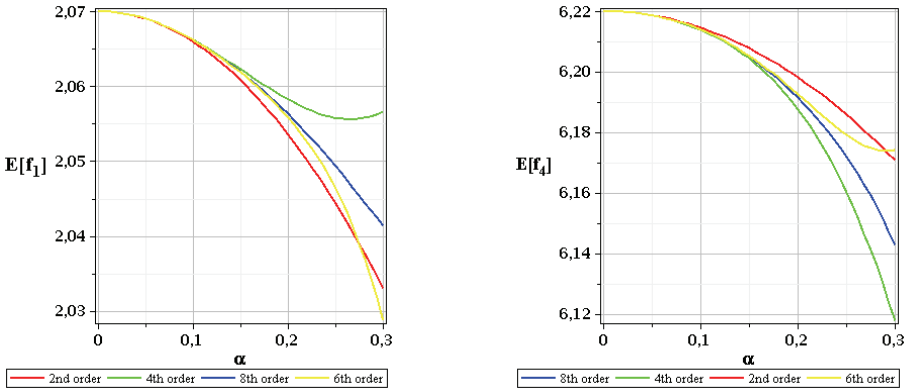

Figure 2: Expected values for first (left) and fourth (right) modes of eigenvibrations

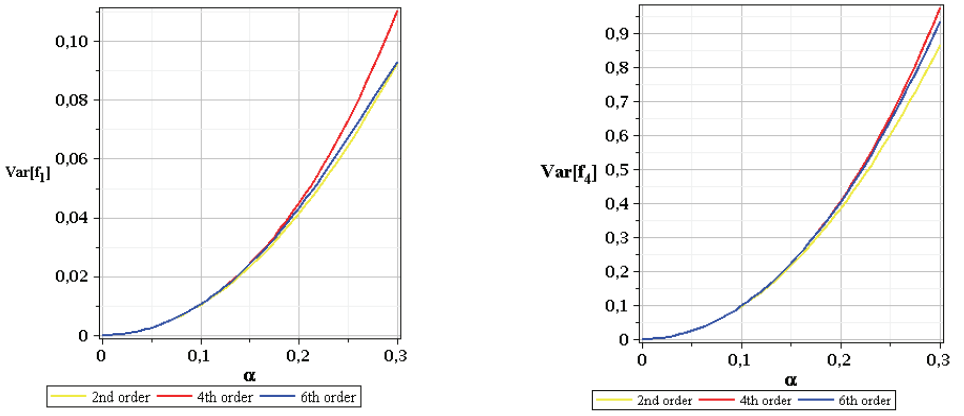

Figure 3: Variances for first (left) and fourth (right) modes of eigenvibrations

(Var[f$_4$], right part of Fig. 3) and for the 2^{nd}, 4^{th} and 6^{th} perturbation orders. Now, the variances have somewhat inverse character than the expectations – although we notice nonlinearity with respect to the input coefficient of variation, but the probabilistic convergence is rather faster in the same input variability interval and these variances increase together with the input coefficient α. It should be underlined that such engineering systems, where an increase of the input uncertainty results in a decrease of the output one are the very exceptional. Moreover, as one may expect, both expected values (after the deterministic counterparts) and the variances increase together with the eigenvalue number. Having further computed third and

fourth central probabilistic moments we recover numerically the skewnesses and kurtosis for the first eigenvibration since the higher modes behave very similarly. They are shown in Fig. 4 (left and right, accordingly) both as the functions of the input coefficient of variation and both in 2^{nd}, 4^{th} and 6^{th} order perturbations (concerning variance approximation in the denominator of Eq. (35)) for $\alpha \in [0.0,0.1]$.

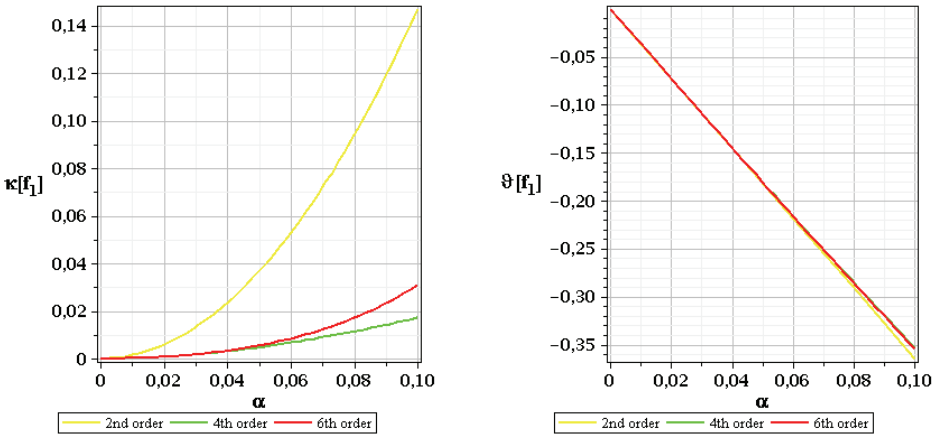

Figure 4: Kurtosis (left) and coefficient of skewness (right) for the first mode of eigenvibrations

Kurtosis – positive everywhere – increases here together with an input α, while skewness – negative for all input values – systematically decreases. As far as kurtosis is highly nonlinear with respect to the input coefficient of variation, skewness is almost linear but both are not independent from the input random dispersion. Further, it is apparent that the skewness stabilizes very fast together with the perturbation order, while kurtosis computed for the orders mentioned above show large variations in-between consecutive orders and needs as high expansion as available. The values of both coefficients are very close to 0, so that one can conclude that the final distribution is quite close to the Gaussian one and, since that, the first two probabilistic moments give sufficient information about the probabilistic response of this tower.

4.2 The tower subjected to random temperature

The second case study is devoted to the influence of the environmental temperature on the internal forces into the structural elements of the telecommunication tower

with the same static scheme as in previous section. This tower is subjected to the same set of external technological loadings, the weight of telecommunication equipment and its dead load. This time a temperature subjected to the structural elements is Gaussian random variable with the expected value equal to $E[T]$=-15˚C and standard deviation being an extra input design parameter in computer analysis. Random thermal elongation is calculated using classical formula $\Delta l = \alpha_T \cdot \Delta T \cdot l_0$, where ΔT is the temperature gradient, α_T stands for the coefficient of thermal expansion and l_0 is the initial element length. Numerical verification is provided using the FEM system ROBOT Structural Analysis 2010 once more jointly with the mathematical package MAPLE, v. 13. An uncertain structural response is verified on two elements – leg in the segment no 9 (see Fig. 5) and the same element type in segment no 5 (in the middle of the total height of the tower). Normal forces are analyzed (their probabilistic moments and coefficients) since they have dominating influence on the overall effort state of the tower elements. The expected values for normal forces in both sections are provided in Fig. 5 as the function of the input coefficient of variation, further we have also the variances for both element locations (cf. Fig. 6) as well as skewnesses and kurtosis (Fig. 7) for the ninth segment element only. Contrary to the previous case study now the variability of the input α is always the same and equal to $\alpha \in [0.0,0.3]$.

Now, the expected values have been computed according to the 2nd up to the 14th stochastic perturbation-based approximations for both structural members. Quite similarly to the eigenvalues, an additional increase of the input coefficient of variation causes the nonlinear decrease of the computed expectations. Quite naturally the normal force mean value in the element located higher is significantly smaller than that located close to the tower foundation (about two and a half times larger) – positive value means a compression here. Although for α>0.15 the results obtained in different theories start to diverge, the vertical axes of both graphs show the changes within the tenths of promiles, so that they are completely negligible.

The variances computed according to the 2^{nd}, 4^{th} and 6^{th} order perturbation methods return practically the same results for the normal forces and almost parabolically increase in case of section 9^{th} and 5^{th} from 0 computed at α=0 (deterministic test). Both kurtosis and skewness shown in left and right graphs of Fig. 7 are determined from the least order approximant of the fourth central moment as well as 2^{nd}, 4^{th} and 6^{th} order variances presented in Fig. 6 – they are computed for the section 9 to see the most transparent differences and tendencies. Now, somewhat contrary to the eigenvibrations analysis, both coefficients have negative values and both decrease together with an increase of the input coefficient α. Even for extremely large maximum random dispersion of a temperature in the range of 30% they are still very close to 0, so that in a presence of random temperature these

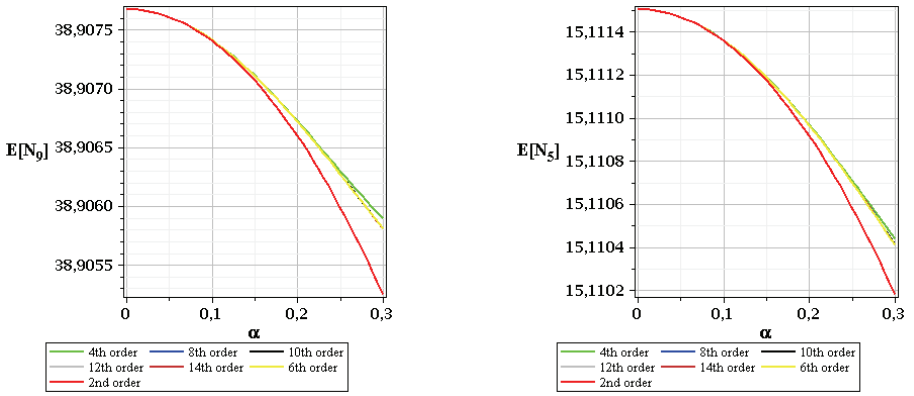

Figure 5: Expected values of normal forces in legs of the tower in section 9 (left) and 5 (right)

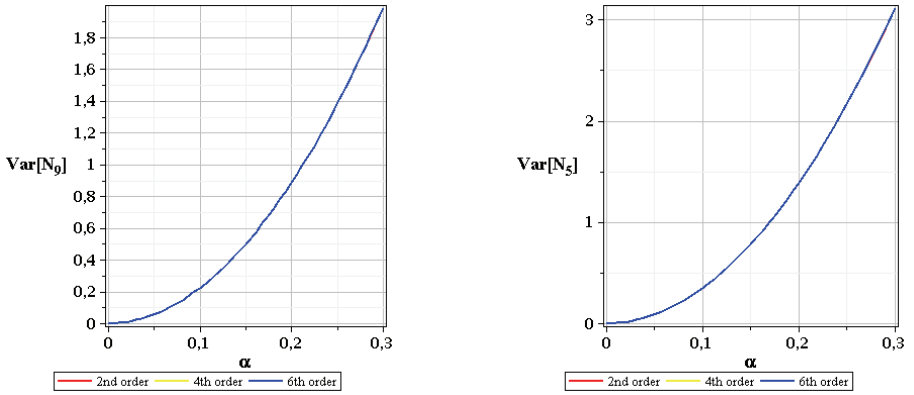

Figure 6: Variances of normal forces in legs of the tower in section 9 (left) and 5(right)

internal forces behave like Gaussian variables. The skewness is practically quite insensitive to the analysis order – there is even no difference on a graph from the initial straight line showing its function with respect to input coefficient of variation. Kurtosis behaviour shows a necessity to drop off the results obtained for the second order, whereas a difference in-between fourth and sixth orders is not so significant, but once more, the highest order is recommended here. It should be mentioned that we assumed here temperature as the random variable for the en-

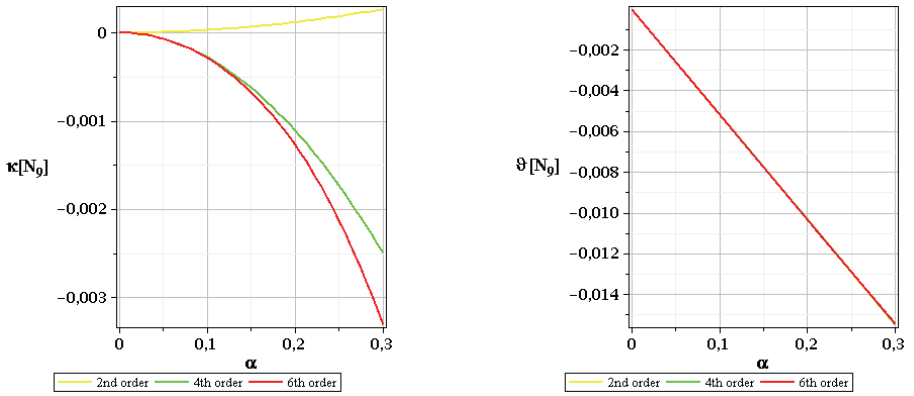

Figure 7: Kurtosis and skewness of normal forces in legs of the tower in section 9 (left) and 5(right)

tire tower having constant value in all the tower's sections; and its non-uniform distribution (convenient for the random fields rather) may bring slightly different results.

4.3 The towers subjected to both ice covers and freezing

Numerical experiments contained in this section deal strictly with determination of an influence of the ice cover thickness on the normal forces in the structural components of the telecommunication towers because it is confirmed with the previous analyses that the influence of the ice covers on the eigenvalues of steel towers without the tensioned cables is definitely not dominating [Wahba et al. (1998)]. It is carried out first on the skeleton analyzed in the section 4.1, while the second tower has 42.0 meters of height and a square cross-section and is shown in Fig. 8. The lower legs of this tower are designed as the thin-walled pipes with the diameters gradually decreasing together with the distance of the cross-section from the foundation level, while the rebars are designed as the full round cross-sections and thin-walled pipes (higher parts) as well as the cold formed channel profiles (lower sections).

The FEM computational model discretized in the system Autodesk Robot Structural Analysis 2011 has been provided using 160 two-noded beam elements and 232 two-noded truss elements joined in 164 nodal points. It needs to be mentioned that the legs are modeled as the continuous beams stiffened by the rebars joined to them with the pins. The internal forces are computed accounting for the self

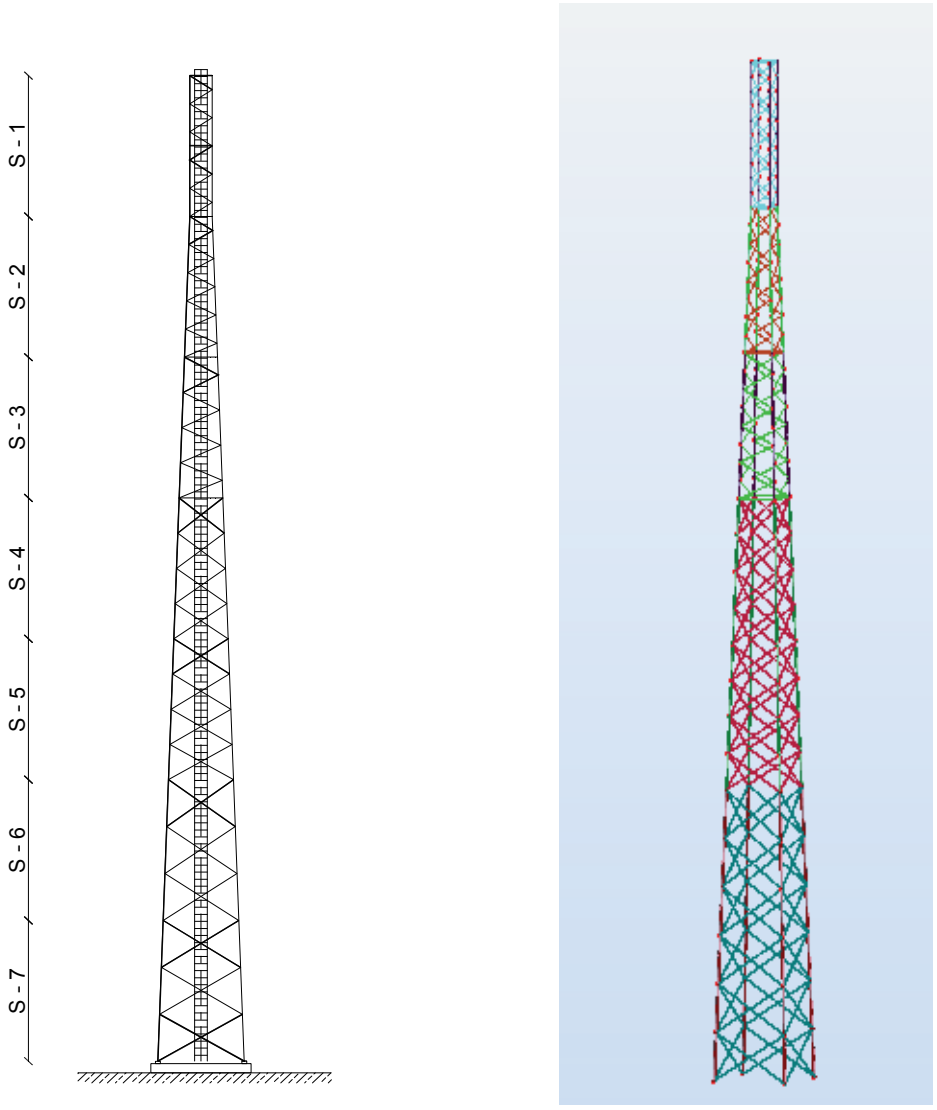

Figure 8: Static scheme and computational model of the tower 42 meters high

weight of structural elements and telecommunication equipment, negative temperature gradients with respect to -15°C as well as the random ice covers' dead load. The thickness of the uniform ice cover was taken from the interval from 0.01 m up to 0.062 m with an increase 0.004 m (14 series of the numerical experiments). To make a clear comparison of the expected values of normal forces (given in kN

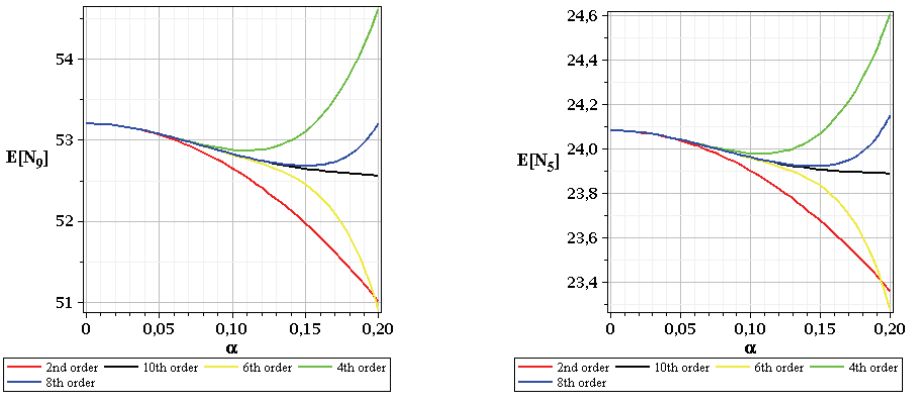

Figure 9: Expected values of normal forces in legs of the tower in section 9 (left) and 5 (right) for first type of the tower

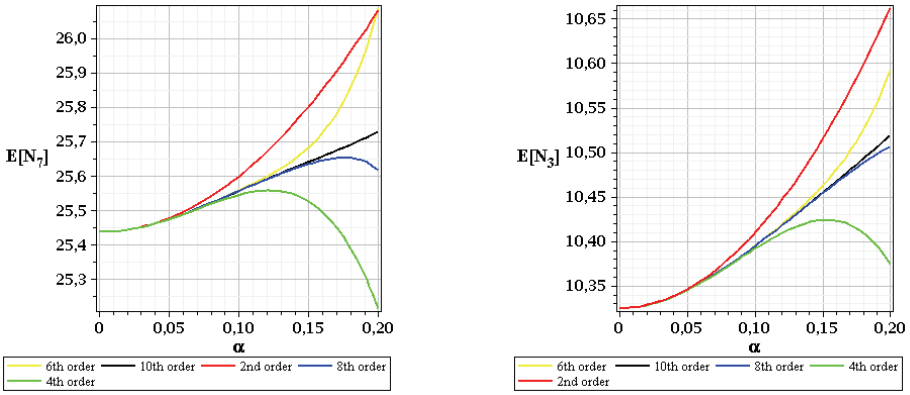

Figure 10: Expected values of normal forces in legs of the tower in section 7 (left) and 3 (right) for second type of the tower

here) in both towers we have taken a single element from the lowest segment and the segment in the middle of the height. These are the ninth and fifth segments correspondingly for higher tower (triangular cross-section) as well as the seventh and third segments for the lower tower; they are all computed as the functions of $\alpha \in [0.0,0.2]$ in the 2^{nd}, 4^{th}, 6^{th}, 8^{th} and 10^{th} stochastic perturbation method orders and presented in Figs. 9-10.

First observation is that the limit value of the input coefficient of variation adequate

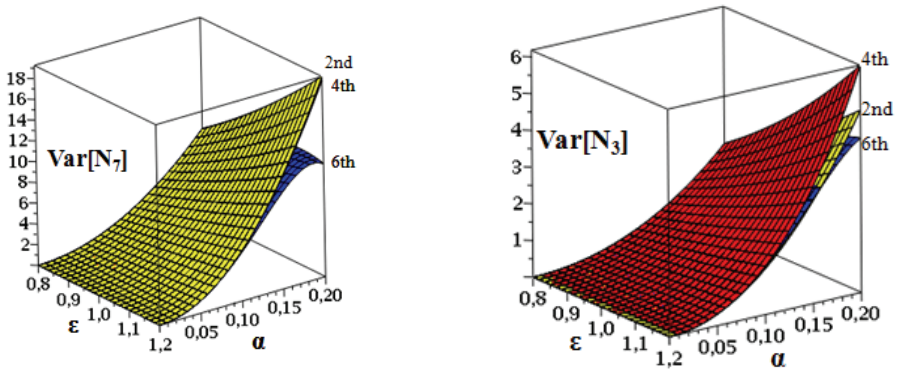

Figure 11: Variances of normal forces in legs of the tower in section 7 (left) and 3(right) for second type of the tower

to a satisfactory agreement of all perturbations orders is significantly smaller in comparison to the previous tests, because even for α=0.10 second order analysis differs from the others. The differences obtained for the same order of analysis and various levels of the input uncertainty is measured in the percents, so that is larger than the numerical modeling error itself. All the graphs show that the tenth order analysis returns the most stable and intermediate results, so that is recommended in further numerical experiments. It is expected after earlier tests that the lower segments show decisively higher compressive forces and stresses (almost more than two times) than the intermediate elements (for both towers). Second interesting observation is that the forces noticed for a greater tower are almost two times larger than these computed for the lower structure but the ratio of their heights is quite far from two – lower tower in this case study appears simply to be significantly more optimal. Next, a comparison of Figs. 9 and 10 shows that an application of the ice covers on all structural elements (which is really the very exceptional case) may result in almost 50% increase of all internal compressive forces and cannot be neglected during all design and verification procedures. Practical observation of these covers shows that only higher elements have significant covers located mostly on the surfaces exposed to the wind blow, while the rest of effective surface and some lower elements remain free from the ice. Finally, it would be very difficult to explain in the theoretical context, why the expectations of normal forces for higher tower decrease all together with the input coefficient of variation, while those computed for lower tower – apparently increase. The variances contained in Fig. 11 are shown in a slightly different manner – with respect to both input coefficient

$\alpha\in[0.0,0.2]$ as well as to the perturbation parameter $\varepsilon\in[0.8,1.2]$ computed as before using 2^{nd}, 4^{th} and 6^{th} order stochastic approaches. This second parameter variability verification is possible due to the hybrid character of the ROBOT-MAPLE interoperability, where analytical expression in ε can be created symbolically. Both variances of the internal forces in lower tower significantly increase together with an additional increase of the parameter α but lower order return larger values than the higher ones. A verification of this methodology gives a lack of sensitivity of these variances with respect to ε at α=0, where the problem is purely deterministic (no perturbation at all). The variances in the middle of the tower related to these in the lowest segment have almost the same ratio as the expectations, so that the output coefficient of variation is a linear combination of the input one. Finally, a sensitivity of the output variances to the input coefficient α is much larger than for the perturbation parameter, where the interrelation is also almost linear. All these surfaces show that the accurate determination of the variances may demand higher even than the sixth order approximations because the differences in-between the orders presented show rather weak convergence.

4.4 Reliability indices for both towers

The first case study in reliability assessment deals with a determination of the index β including the induced and free vibrations frequencies of the tower, analyzed probabilistically in Sec. 4.1 (the highest structure), where the limit function is defined as a difference in-between the forced ω_{for} as well as the eigenvibrations ω_{nat}. We have studied four cases with the differences relevant to 15, 25, 30 and 35% of the eigenfrequency; of course, an increase of this difference systematically decreases a probability of the structural failure here, so that the reliability index should automatically increase. Computational results of this analysis (with the reliability indices computed symbolically in the system MAPLE) are presented in Fig. 12 as the functions of the input coefficient of variation α. The horizontal axis has been shortened to α=[0.05,0.21] for a brevity of the presentation. Let us remind also that the values of the reliability indices corresponding to the lower safety limits belong to the interval $\beta \in [3.0;5.0]$.

According to our explanation given above, the indices are inversely proportional to the input uncertainty level and one concludes that the larger difference of both frequencies, the higher reliability of the tower. Comparing specific numerical data given here we need to disqualify 15% difference resulting in the index equal and smaller than 4 as inappropriate according to Eurocode 0. The margin of 25% is much better, however until α=0.065, which may be quite unrealistic considering the wind nature; the best situation is for 35% difference, where α=0.085 is allowable. A negative verification of this index for the newly erected realistic structure does

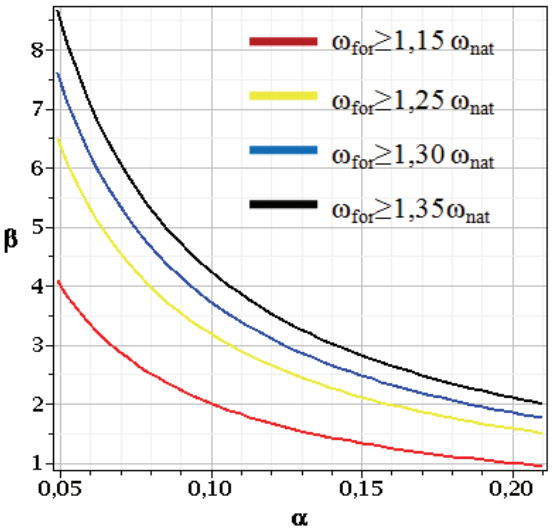

Figure 12: Reliability indices for the eigenvibrations for the 52,0 m high tower

not mean automatically a serious probability of a danger – as one may conclude the new Eurocodes, especially in the context of the reliability issues – are simply much more restrictive than the traditional deterministic designing procedures known before. The second part of reliability verification devoted to maximum horizontal deflection and a rotation has been provided on the basis of the lowest tower (40.5 meters high given in Fig. 13) discretized with 45 two-noded beam elements and 106 two-noded bar elements joined in 48 nodes in the system ROBOT. According to the statements of Eurocode no 1, we included into the final magnitude of this load the exposition coefficient, aerodynamic resistance factor, while the wind speed q was treated here as the Gaussian random variable with three different mean values affecting the reliability index: (a) q_1= 0,30 kN/m^2 (adjacent to 79,2 km/h), (b) q_2= 0,40 kN/m^2 (for 105,6 km/h) and (c) q_3= 0,50 kN/m^2 (in case of 132,0 km/h).

Since our computational procedure is based on the recovery of the response functions for some variations of the input random variable around its mean value, we have taken the following wind speed intervals: (a) for q_1=0,30 kN/m^{2}in the range from 0,22kN/m^2 until 0,38 kN/m^2, (b) for q_2=0,40 kN/m^2 in the range from 0,32kN/m^2 until 0,48 kN/m^2 and, finally (c) for q_3=0,50 kN/m^2 within an interval from 0,42kN/m^2 up to 0,58 kN/m^2 – all having the basic interval of 0,02 kN/m^2. The following assumptions accompanied the reliability index determination: (a) maximum horizontal deflection is taken as 40,5 cm (as a single percent of its

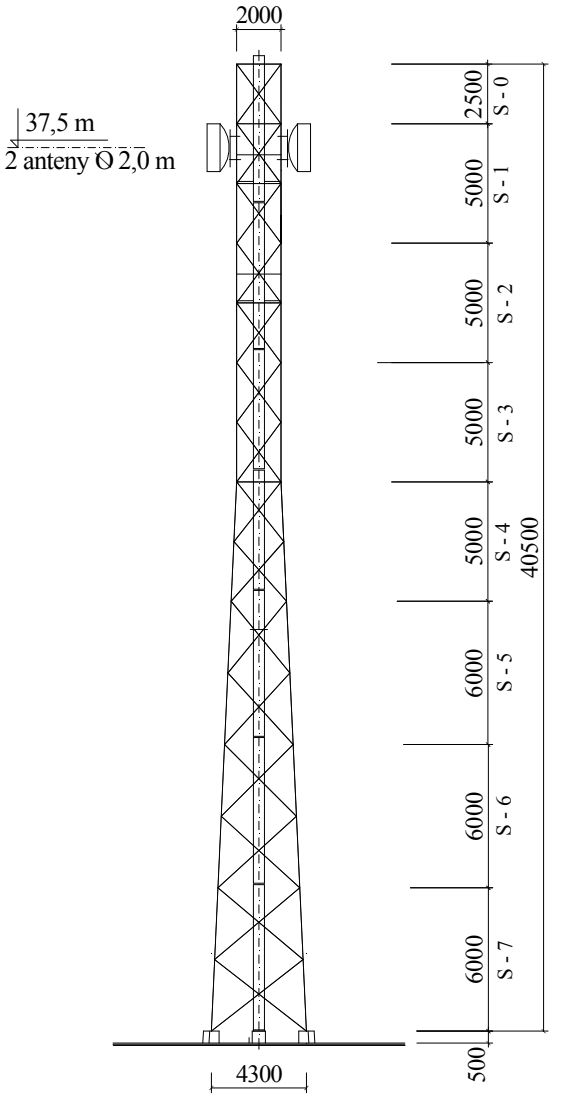

Figure 13: Static scheme of the 42 meters high tower

height), (b) standard deviation of this deflection equals to 5% of this mean – 2,025 cm, (c) maximum allowable rotation is adopted as 1°, (d) its standard deviation is once more equal to – 5% (0,05°). All reliability indices have been determined for various mean wind speeds: (a) β_{1U} and β_{1R} – for 0,30 kN/m^2 (U stands for maximum deflection here and R denotes a rotation), (b) β_{2U} and β_{2R} – in case of 0,40

kN/m^2 and, finally, (c) β_{3U} as well as β_{3R} – both for 0,50 kN/m^2.

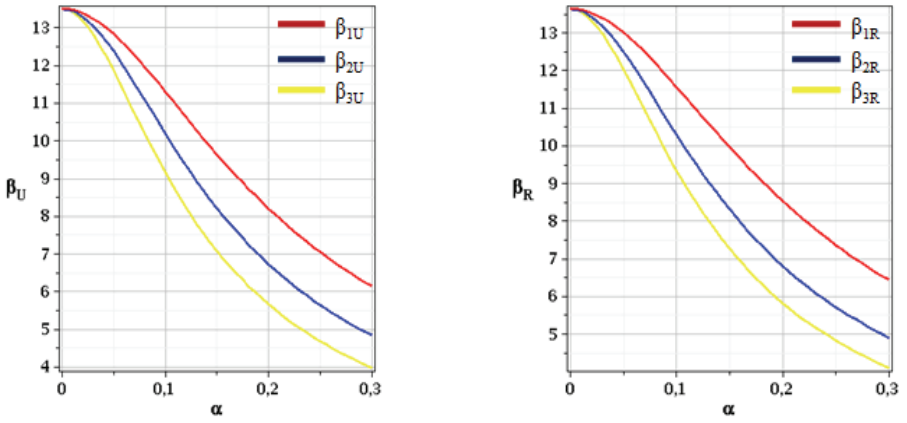

Figure 14: Reliability index for the maximum horizontal deflection (left) and rotation (right)

Fig. 14 contains the curves representing the functions of the reliability index for the maximum horizontal deflection of the tower analyzed (β_U) and, separately, for their maximum rotation around its vertical symmetry axis (β_R) also presented with respect to the input uncertainty. The largest values are computed for the lowest wind speeds ($\beta_{1U,}$ β_{1R}), which gives some confirmation of this model as the structure is the most safe for the smallest wind action. An initial value for this index corresponding to the deterministic problem (as input α=0) is almost three times larger than the maximum allowable values contained in Eurocode 0 and even for α=0.3 (maximum random dispersion of the wind blow) the smallest wind pressure is adequate to the safe state of the tower. The shapes of all curves are very similar to each other and accidentally close to the bell shaped curve with different flatness ratios. Of course, the higher wind speed, the smaller overall reliability index, so that for the second case study and close to α=0.3 we can fall into the failure region, whereas the third, largest speed may cause this failure shortly after α=0.22. It is very interesting indeed, that both limit states – for displacements and rotations – result in almost the same values of the reliability indices and it may mean that the tower is really optimized concerning a spatial distribution of the structural elements. Nevertheless, a general conclusion from this verification is that the telecommunication towers are highly sensitive to the wind speed (modeled usually as the equivalent static pressure) and may be relatively easy subjected to the catastrophic

failure for the hurricanes classified into the third category (178-209 km/h) in the Saffire-Simpson classification.

5 Concluding remarks

1. The generalized stochastic perturbation technique implemented as the Stochastic Finite Element Method presented in this paper enables for the hybrid FEM-symbolic determination and visualization of up to the fourth order probabilistic moments and probabilistic coefficients as well as the reliability indices according to both FORM and SORM (in the nearest future). Its application for the eigenfrequencies and internal forces analysis in the steel telecommunication towers shows that for most of the Gaussian random input parameters the structural response has also Gaussian PDF, so that really first two-moments information about the output is necessary. Computational experiments performed with the stochastic ice covers on the structural elements shows that this atmospheric loading may be extremely dangerous in civil engineering practice and cannot be disregarded during a designing process for these type of structures, leading to about 50% increase of the internal forces and having no larger influence on the eigenvibrations expectations. Numerical experiments with the reliability indices driven by the wind blow and based on the structural deformations show that the current regulations of the Eurocode 0 are significantly more restrictive than the previous deterministic codes, because the existing structures correct from the older codes viewpoint may be on the limits of the safe exploitation according to the new rules.

2. Further works with a computational implementation of the generalized perturbation-based stochastic finite element method should undoubtedly focus on the multi-parametric input randomness, because a combination of the correlated various sources may enormously increase the output uncertainty completely changing the functions of the reliability indices studied here as the single parameter functions; the same comment remains true for non-Gaussian variables [Kamiński and Szafran (2009)]. Another interesting engineering problem would be a computational sensitivity analysis of steel telecommunication towers to some geometrical imperfections [Jia and Mang (2011)], that may appear and can be especially dangerous for the large scale structures. Finally, the earthquake resistance of the steel telecommunication towers will be verified since further extensions of the stochastic computer technique presented on the structural forced vibrations with random parameters and random time series.

Acknowledgement: This paper has been financially supported by the Polish National Science Center under the grant no 519 386 636.

References

Bathe, K.J. (1996): *Finite Element Procedures*. Prentice Hall, Englewood Cliffs, New York.

Bendat, J.S., Piersol, A.G. (1971): *Random Data: Analysis and Measurement Procedures*. New York, Wiley.

Benaroya, H. (1992): Random eigenvalues, algebraic methods and structural dynamic models. *Appl. Math. Comput.*, vol. 37, no. 1, pp. 66-52.

Boswell, M.T. et al. (1993): *The Art of Computer Generation of Random Variables*. In: *Handbook of Statistics*, Vol. 9: *Computational Statistics*. Amsterdam, Elsevier.

Chen, J.B., Li, J. (2005): Dynamic response and reliability analysis of non-linear stochastic structures. *Prob. Engrg. Mech.*, vol. 20, no. 1, pp. 33-44.

De Oliveira, M.I.R. et al. (2007): Structural analysis of guyed steel telecommunication towers for radio antennas. *J. Brazilian Soc. Mech. Sci. Engrg.*, vol. 29, no. 2, pp. 185-195.

De Oliveira, M.I.R. et al. (2005): Structural assessment of current steel design models for transmission and telecommunication towers. *J. Constr. Steel Res.*, vol. 61, no. 8, pp. 1108-1134.

El-Fashny, K., Chouinard, L.E., McClure, G. (1999): Reliability analysis of a telecommunication tower. *Canadian J. Civ. Engrg.*, vol. 26, no. 1, pp. 1-12.

Elishakoff, I. (1983): *Probabilistic Methods in the Theory of Structures*. New York, Wiley-Interscience.

Fengli, Y., Jingbo, Y., Junke, H., Jie, F.D. (2010): Dynamic responses of transmission tower-line system under ice shedding. *Int. J. Struct. Stability & Dyn.*, vol. 10, no. 3, pp. 461-481.

Hughes, T.J.R. (2000): *The Finite Element Method – Linear Static and Dynamic Finite Element Analysis*. New York, Dover Publications, Inc.

Jia, X., Mang, H.A. (2011): Conversion of imperfection-sensitive elastic structures into imperfection-insensitive ones by adding tensile members. *J. Int. Assoc. Shell. Spatial Struct.*, vol. 52, no. 2, pp. 121 – 128.

Kamiński, M. (2005): *Computational Mechanics of Composite Materials*. London – New York, Springer-Verlag.

Kamiński, M. (2009): Generalized stochastic perturbation technique in engineer-

ing computations. *Math. Comp. Model.*, vol. 51, no. 3-4, pp. 272-285.

Kamiński, M. (2011): Probabilistic analysis of transient problems by the least squares stochastic perturbation-based finite element method. *CMES: Computer Modeling in Engineering & Sciences*, vol. 80, no. 1, pp. 113-140.

Kamiński, M., Szafran, J. (2009): Eigenvalue analysis for high telecommunication towers with lognormal stiffness by the response function method and SFEM. *Comput. Ass. Mech. Engrg. Sci.*, vol. 16, pp. 279-290.

Khan, M.A., Siddiqui, N.A., Abbas, H. (2004): Reliability analysis of latticed steel towers against wind induced displacement. *Steel & Compos. Struct.*, vol. 4, no. 1, pp. 9-21.

Kleiber, M., Hien, T.D. (1992): *The Stochastic Finite Element Method*. Chichester,Wiley.

Lin, Y.K. (1967): *Probabilistic Theory of Structural Dynamics*. New York, McGraw-Hill.

Melchers, R.E. (1999): *Structural Reliability. Analysis and Prediction*. 2nd edition. Chichester, Wiley.

Nielsen, M.G. (2009): The analysis of masts and towers. *Int. J. Space Struct.*, vol. 24, no. 2, pp. 97-102.

Ohkubo, J., Eggel, T. (2011): A direct numerical method for obtaining the counting statistics for stochastic processes. *J. Stat. Mech.: Theory Exp.*, vol. 6, art. no. P06013.

Pradlwater, H.J., Schueller, G.I., Szekely, G.S. (2002): Random eigenvalue problems for large systems. *Comput. & Struct.*, vol. 80, no. 27, pp. 2415-2424.

Schueller, G.I., Pradlwater, H.J. (2009): Uncertain linear systems in dynamics: Retrospective and recent developments by stochastic approaches. *Engrg. Struct.* , vol. 31, no. 11, pp. 2507-2517.

Śniady, P., Żukowski, S. (1988): Static probabilistic analysis of frame structures. *Arch. Civ. Engrg.*, vol. 34, no. 2, pp. 175-189.

Wahba, Y.M.F., Madugla, M.K.S., Monforton, G.R. (1998): Effect of icing on the free vibration of guyed antenna towers. *Atmospheric Res.*, vol. 46, pp. 27-35.